PHYSICAL REVIEW B **91**, 104519 (2015)

Superconductivity and role of pnictogen and Fe substitution in 112-LaPd$_x$*Pn*$_2$ (*Pn* = Sb, Bi)

Reiner Retzlaff,[1] Alexander Buckow,[1] Philipp Komissinskiy,[1] Soumya Ray,[1] Stefan Schmidt,[2] Holger Mühlig,[2]
Frank Schmidl,[2] Paul Seidel,[2] Jose Kurian,[1] and Lambert Alff[1,*]
[1]*Institute of Materials Science, Technische Universität Darmstadt, Alarich-Weiss-Strasse 2, 64287 Darmstadt, Germany*
[2]*Institut für Festkörperphysik, Friedrich-Schiller-Universität Jena, Helmholtzweg 5, 07743 Jena, Germany*
(Received 8 January 2015; revised manuscript received 6 March 2015; published 26 March 2015)

We report on the epitaxial growth of As-free and phase-pure thin films of the 112-pnictide compounds LaPd$_x$$Pn_2$ (Pn = Sb, Bi) grown on (100) MgO substrates by molecular beam epitaxy. X-ray diffraction, reflection high-energy electron diffraction, and x-ray photoelectron spectroscopy confirm the HfCuSi$_2$ structure of the material with a peculiar pnictogen square net layer. The superconducting transition temperature T_c varies little with Pd concentration. LaPd$_x$Sb$_2$ has a higher T_c (3.2 K) by about 20% compared with LaPd$_x$Bi$_2$ (2.7 K). Fe substitution of Pd leads to a rapid decay of superconductivity, suggesting that these superconductors are conventional type II.

DOI: 10.1103/PhysRevB.91.104519 PACS number(s): 74.70.Dd, 74.70.Xa, 74.78.−w, 81.15.Hi

I. INTRODUCTION

The research on Fe-based pnictides with ZrCuSiAs structure [1] has led to the discovery of materials with superconducting transition temperatures T_c as high as 56 K [2–4]. In these compounds the pnictogen is arsenic or phosphor. It is desirable to search for As-free superconducting pnictides not only because of the highly toxic nature of this element but also because of fundamental interest in understanding the role of the pnictogen ion by investigating, e.g., Bi- and Sb-based compounds. There are predictions that the substitution of As by Sb could even lead to novel high-temperature superconductors [5,6]. While the vast majority of research has focused on the 1111-, 122-, 111-, and 11-type pnictides and chalcogenides, recently, high-transition temperatures of up to 45 K have also been reported in the 112-type iron pnictides Ca$_{1-x}$La$_x$FeAs$_2$, with x between 0.1 and 0.2 [7–11]. One modification of the 112 structure belongs to the same symmetry group $P4/nmm$ (No. 129) as the 1111- or ZrCuSiAs-type materials. However, the atomic arrangement contains a peculiar pnictogen square net layer that was identified for the first time for the compound HfCuSi$_2$ in 1975 [12,13]. Sometimes, this structure type is also referred to as ZrCuSi$_2$ (which is easily confused with ZrCuSiAs). Recently, in this modification of the 112 type, superconductivity has been discovered at about 4 K in RENi$_x$Bi$_2$, with RE = La, Ce, Nd, and Y [14]. One intriguing property of these compounds is the mixed-valence state of the pnictogen. In the pnictogen square net layer, the ions have a formal valence of −1, while in the more three-dimensional metal-pnictogen layer (corresponding to the Fe-As layer, e.g., in LaFeAsO) the pnictide has a formal valence of −3. For most rare-earth elements it is difficult to achieve phase-pure bulk materials with a large superconducting volume fraction in RENi$_x$$Pn_2$ [14]. In the case of CeNi$_{0.8}$Bi$_2$, samples suitable for neutron scattering were achieved, revealing that the antiferromagnetic ordering of Ce^{3+} does not interact with the superconducting condensate. The missing coupling of spin fluctuations to the superconducting charge carriers has been interpreted as the reason for the low critical temperature in this compound [15]. Recently, it has been argued along the same lines that the isostructural compound HfCuGe$_2$ is a nonmagnetic analog of the 1111 iron pnictides and therefore has a reduced T_c of 0.6 K [16]. Kodama *et al.* have suggested that superconductivity occurs in the pnictogen square net layer instead of the transition-metal-pnictogen layer [15]. Recently, the Pd-based compounds LaPd$_{1-x}$Bi$_2$ and CePd$_{1-x}$Bi$_2$ have been grown as single crystals, with a bulk T_c of 2.1 K for LaPd$_{1-x}$Bi$_2$, whereas CePd$_{1-x}$Bi$_2$ was nonsuperconducting with antiferromagnetic ordering at 6 K [17]. Note that the previously mentioned high T_c values above 34 K have been achieved in a second modification of the 112 type which is distorted from the space group $P4/nmm$ to the monoclinic space group $P2_1$ (No. 4) [7–9]. Nevertheless, the key structural features of the quasi-two-dimensional square net layer where As bonds are arranged in a zigzag way and the typical Fe-pnictide layer common to all pnictide superconductors are the same for both modifications. We stress that the reported high T_c values still await confirmation.

Some of the difficulties in preparing bulk samples of 112 type can be overcome by using a thin-film approach [18,19]. It has been reported for CeNi$_x$Bi$_2$ and LaNi$_x$Bi$_2$ that phase-pure epitaxial thin films with T_c similar to or even higher than those of the bulk can be prepared by molecular beam epitaxy (MBE) [20,21]. For antimonides, superconducting transitions have been reported for LaNi$_x$Sb$_2$ at 1.0 K, for LaCu$_x$Sb$_2$ at 0.9 K, and for LaPd$_x$Sb$_2$ at 2.7 K [22]. The 112 compounds tend to have a relatively large amount of metal vacancies (indicated by $x < 1$) due to the formal valence state of −1, which is partially avoided by vacancy formation. With respect to the role of Sb, it is interesting to note that slight Sb doping into Ca$_{1-x}$La$_x$FeAs$_{0.99}$Sb$_{0.01}$ with $x = 0.15$ has induced a higher T_c [9]. Recently, several studies of the Pd-based 122 compounds APd$_2$As$_2$ (A = Ca, Sr, Ba, La) and SrPd$_2$Ge$_2$ have shown that they are conventional type-II nodeless (but anisotropic) s-wave electron-phonon superconductors with a maximum T_c of 1.4 K [23–25]. Since it is difficult to stabilize the Fe-based 112 bismuthides and antimonides [26], we have investigated epitaxial thin films of LaPd$_x$Sb$_2$ and LaPd$_x$Bi$_2$ to study the role of the pnictogen ion. In addition, we have

---

[*] alff@oxide.tu-darmstadt.de

studied the role of Fe by substituting up to half of the Pd in La$(\mathrm{Pd}_{1-y},\mathrm{Fe}_y)_x\mathrm{Sb}_2$ with $0 \leqslant y \leqslant 0.5$.

II. EXPERIMENT

Thin films were grown by MBE in a custom-designed ultrahigh-vacuum (UHV) chamber with a base pressure of about 10^{-9} mbar. The chamber was equipped with three electron evaporation guns and separate collimated quartz-crystal microbalance (QCM) sensor heads for rate monitoring in a feedback loop to the e-guns controlled by a state-of-the-art four-channel thin-film deposition controller (Cygnus, Inficon). In addition, a high-temperature effusion cell was used. For thin-film growth, elemental metal sources are simultaneously coevaporated (La, Lesker 99.9%; Pd, ChemPur, 99.95%; Sb, ChemPur, 99.999%; Bi, ChemPur, 99.999%). As a substrate material we have chosen (100) MgO preannealed at 800 °C for 10 h in air in an external furnace [27]. After deposition, the films were cooled in UHV below 150 °C before being exposed to atmosphere for further characterization. The structural characterization was carried out by x-ray diffraction (XRD; Rigaku, SmartLab) with monochromatic Cu K_α radiation. Electronic transport measurements were performed in an Oxford ^{3}He cryostat using a four-probe technique, and the magnetization was measured in a superconducting quantum interference device (SQUID; MPMS, Quantum Design). X-ray photoelectron spectroscopy (XPS) measurements were conducted with monochromatic Al K_α radiation using a PHI Versaprobe 5000 spectrometer. The experimental energy resolution of the spectrometer of 0.3 eV was determined from the Gaussian broadening of the Fermi edge of a sputter-cleaned Ag reference sample.

III. RESULTS AND DISCUSSION

A. LaPd$_x$Sb$_2$

The LaPd$_x$Sb$_2$ thin films were grown in the temperature range between 440 °C and 520 °C with a typical growth rate of 0.5 Å/s. The desired structure formed in this temperature window of 80 °C. Lower growth temperatures resulted in polycrystalline films, whereas higher temperatures resulted in Sb deficiency. This deficiency can be compensated by increasing the deposition rate at higher temperatures. However, the crystallinity of the thin films is best around 480 °C. At optimal conditions the films grow epitaxially on (100) MgO with a smooth and atomically flat surface, as can be seen in the clear, streaky reflection high-energy electron diffraction (RHEED) pattern shown in Fig. 1.

The thin films are phase pure, and out-of-plane 2θ-ω x-ray scans indicate a pure c-axis orientation. No impurity phases are detected by XRD. A typical 2θ-ω scan is shown in Fig. 2. All peaks correspond to $(00l)$ reflections, demonstrating the single-phase nature of the films. From the XRD pattern the c-axis lattice parameter was determined using the Nelson-Riley method [28]. The extrapolated value of $c = 9.88(5)$ Å is a bit smaller than the reported bulk values in the literature of $c = 9.982$ Å [22]. For optimal growth conditions, Laue oscillations can be observed (see the right inset in Fig. 2), indicating coherent growth and allowing the determination of the film thickness. The determined thickness of $t_{\mathrm{Laue}} =$ 25.7 nm is in good agreement with the analysis of the x-ray reflection (XRR) measurements (see left inset in Fig. 2), giving $t_{\mathrm{XRR}} = 26.1$ nm. The best rocking curves have a FWHM of about 0.03°–0.05°. The a-axis lattice parameter of LaPd$_x$Sb$_2$ is 4.52(2) Å, resulting in a lattice mismatch to the MgO substrate of 7.4%.

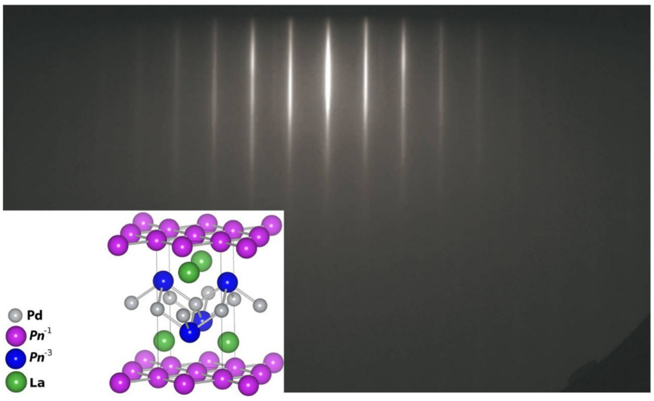

FIG. 1. (Color online) Room-temperature RHEED pattern of LaPd$_x$Sb$_2$ with the beam azimuth in the ⟨100⟩ direction of the MgO substrate. The streaks indicate atomically smooth and epitaxial growth. The inset shows a sketch of the crystal structure.

In order to determine the in-plane texture and the epitaxial relation of the LaPd$_x$Sb$_2$ thin films on MgO substrates, x-ray ϕ scans were carried out. Typical ϕ scans of the (112) reflection of the thin film and the (111) reflection of the MgO substrate are shown in Fig. 3. Because of the fourfold symmetry of the tetragonal structure a set of four peaks with 90° spacing is expected. Exactly in between these peaks, an additional set of four peaks with reduced intensity is observed. This indicates that two domains are formed with one domain rotated by 45° with respect to the other. From the online observation of the RHEED patterns one can conclude that during the growth of the first unit cells both domains are present. In the later growth

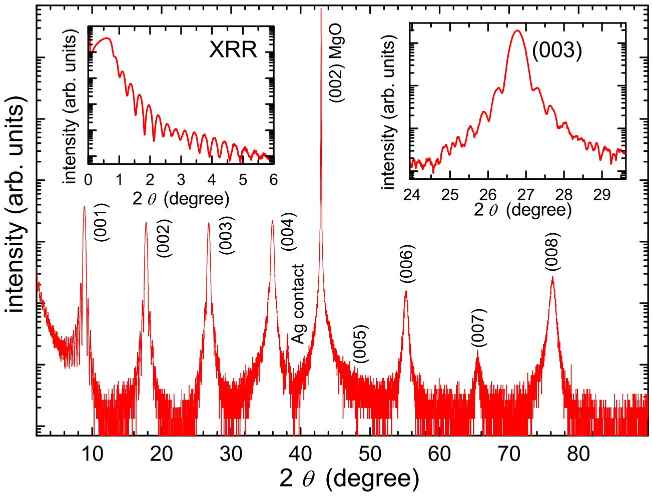

FIG. 2. (Color online) A 2θ-ω XRD scan of LaPd$_x$Sb$_2$. The intensities are shown on a logarithmic scale. The left inset shows an XRR measurement, and the right inset shows a zoom of the (003) reflection.

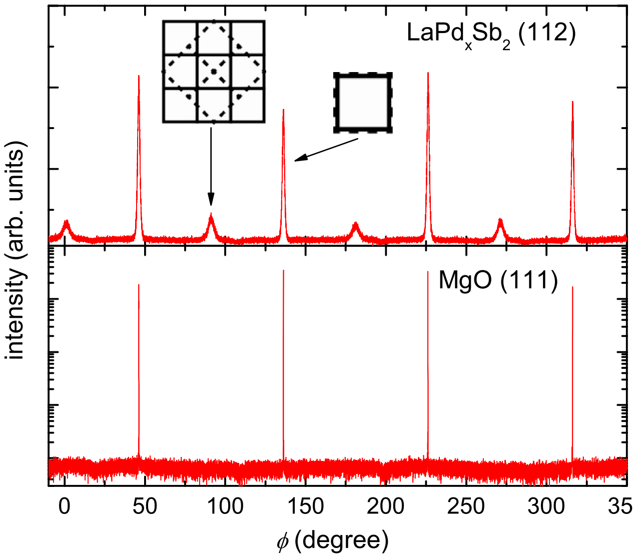

FIG. 3. (Color online) ϕ scans of the LaPd$_x$Sb$_2$ (112) reflection and MgO (111) reflection. The drawings represent the two epitaxial relations. The dashed cube is the LaPd$_x$Sb$_2$ (112) unit cell; the solid line represents the MgO unit cell.

stage, only the major nonrotated domain remains. The rotated domain therefore occurs only at the interface with the substrate and, subsequently, is overgrown by the majority domain. The interface energy difference for unrotated and rotated growth seems to be small and is governed by the surface conditions of MgO. On as-received substrates, the rotated growth is favored, while vacuum annealing at 800° leads to cube-on-cube growth. The drawings in Fig. 3 suggest an epitaxial relation for the rotated domain (2×2 on rotated 3×3 unit cells) with a lattice mismatch of only 1.2%.

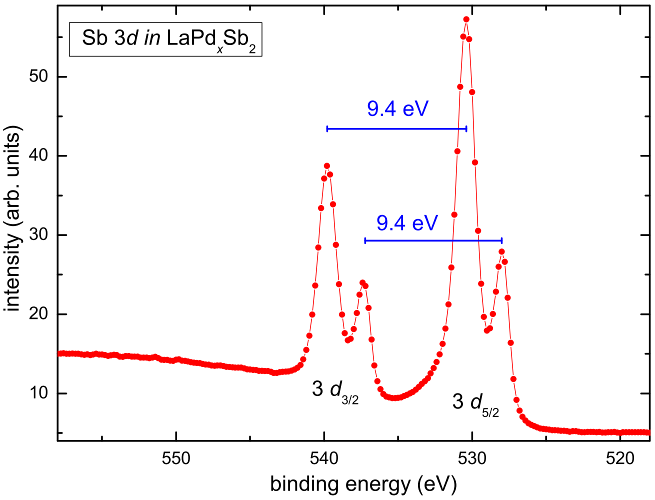

FIG. 4. (Color online) XPS spectra of the Sb $3d$ core level in LaPd$_x$Sb$_2$. The two larger peaks correspond to Sb^{-3}; the smaller peaks correspond to Sb^{-1}.

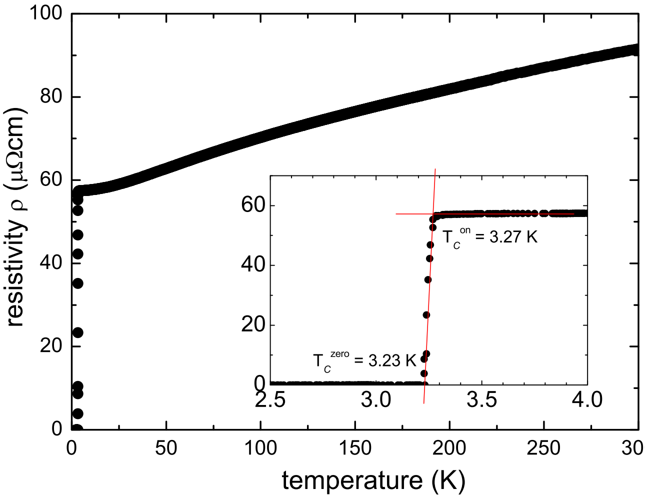

FIG. 5. (Color online) Temperature dependence of the resistivity of a LaPd$_x$Sb$_2$ thin film.

The pnictide ions in the 112 compounds occur in two different oxidation states at different positions in the unit cell. Figure 4 shows the XPS spectra of the Sb $3d$ core level of a LaPd$_x$Sb$_2$ thin film measured with Al K_α radiation. Antimony has two $3d$ photoelectron lines due to the spin-orbit interaction, and they are separated by $\Delta = 9.4$ eV. The spectra clearly show two doublets representing the two valence states. The more intensive lines at higher energies correspond to the oxidation state Sb^{-3}; the second peak can be attributed to the Sb^{-1} state within the square net layer.

We have measured the electrical properties of LaPd$_x$Sb$_2$ using a four-point resistivity measurement. The resistivity vs temperature behavior is shown in Fig. 5. The thin film has a room-temperature resistivity of $\rho(300\,\mathrm{K}) = 91.5\,\mu\Omega$ cm and a residual resistivity ratio of $\rho(300\,\mathrm{K})/\rho(10\,\mathrm{K}) = 1.58$. The data show a sharp superconducting transition with $T_c^{\mathrm{onset}} = 3.27$ K and $T_c^{\mathrm{zero}} = 3.23$ K. The transition width defined by the 90/10 criterion is $\Delta T = 0.03$ K. In the range of 5 K to about 30 K, the resistivity shows a metallic behavior with a quadratic $\rho(T) = \rho_0 + AT^2$ dependence with $\rho_0 = 57.4\ \mu\Omega$ cm and $A \approx 2.54\ \mathrm{n}\Omega\,\mathrm{cm/K}^2$. Between 30 K and room temperature a rather linear or even convex behavior is found. We have also measured magnetization vs temperature using a SQUID in a field of 8 Oe applied perpendicular to the thin-film plane. The data clearly show the onset of the Meissner shielding at 2.9 K, confirming a superconducting phase with significant volume. The low-field scan of the magnetization at 1.8 K had a typical shape of a type-II superconductor with a lower critical field $H_{c1} = 10$ Oe (corresponding to 1 mT). Figure 6 shows the field dependence of the superconducting transition in LaPd$_x$Sb$_2$. The magnetic field was applied perpendicular to the sample surface. The midpoint of the superconducting transition shifts from 2.90 K at 0 T to 1.78 K at 0.5 T. A rough extrapolation of the decrease of the superconducting transition temperature leads to an estimated upper critical field of about $H_{c2} = 1.1$ T.

We have investigated the influence of the Sb and Pd concentration in LaPd$_x$Sb$_2$. The Sb concentration has almost no influence on the critical temperature. In the range of ±5% of Sb variation, the critical temperature remains constant. For larger deviations, the superconductivity is immediately destroyed, along with a strong decline in crystallinity. The influence of the Pd variation is shown in Fig. 7. The

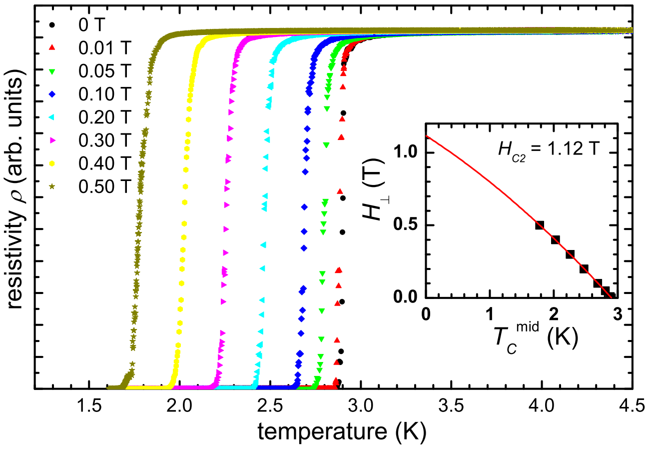

FIG. 6. (Color online) Superconducting transition of a $LaPd_xSb_2$ thin film shown for different magnetic fields applied perpendicular to the film surface. The inset shows the extrapolation of the critical field vs transition temperature behavior.

critical temperature shows a broad dome-shaped behavior as a function of Pd concentration. At the edges of the dome, the superconductivity rapidly vanishes, accompanied by a strong decrease in sample quality. We have calculated the expected deposition rate for perfect stoichiometry in $LaPdSb_2$ ($x = 1$) from an inductively coupled plasma analysis (ICP). Interestingly, the superconductivity breaks down before this point is reached, and the crystallinity is strongly worsened. We conclude from these observations that the main reason for the degradation of the superconducting state is the lattice destabilization instead of some kind of doping effect.

B. $LaPd_xBi_2$

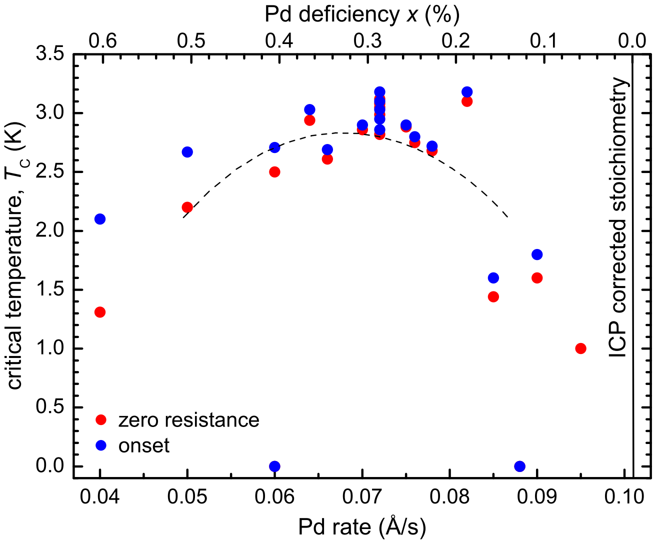

FIG. 7. (Color online) Phase diagram of $LaPd_xSb_2$ showing the critical temperature vs Pd content. Onset and zero-resistance values are shown. The line on the right corresponds to $LaPdSb_2$ as calculated from ICP data. The dashed line is a guide to the eye.

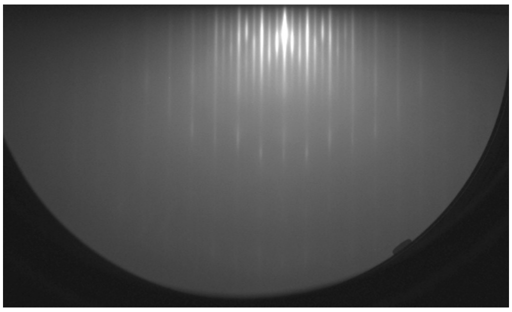

FIG. 8. RHEED pattern from the surface of a $LaPd_xBi_2$ thin film with beam azimuth in the ⟨110⟩ direction of MgO. The streaks indicate atomically smooth and epitaxial growth.

$LaPd_xBi_2$ can be grown on MgO substrates under conditions similar to those for $LaPd_xSb_2$. However, the substrate temperature range for the Bi-based compound is narrower than that for the Sb-based compound. For $LaPd_xBi_2$ the growth window is between 405 °C and 445 °C, similar to the one for $LaNi_xBi_2$ and $CeNi_xBi_2$ [20,21]. The bismuth compound $LaPd_xBi_2$ is not stable in air. The samples degrade fast, which makes characterization challenging. With the optimal growth conditions the films grow epitaxially on (100) MgO with a smooth and atomically flat surface, as can be deduced from the streaky RHEED pattern shown in Fig. 8. The electron-beam azimuth is in the ⟨110⟩ direction of MgO. The additional fine lines between the main streaks indicate a surface reconstruction which has not been observed for the Sb-based compound.

The $LaPd_xBi_2$ thin films are phase pure, and the out-of-plane 2θ-ω x-ray scans show a c-axis orientation. A typical 2θ-ω scan is shown in Fig. 9. All peaks correspond to $(00l)$ reflections, indicating the single-phase nature of the film. The c-axis lattice parameter extrapolated by the Nelson-Riley method is $c = 9.70(9)$ Å. Calculated from the RHEED pattern, the a-axis lattice constant is about $a = 4.55$ Å. The best FWHM values of the rocking curve of the (003) reflection are about $0.05(4)^\circ$. Additionally, there is a broad background from diffuse scattering due to dislocations with a FWHM

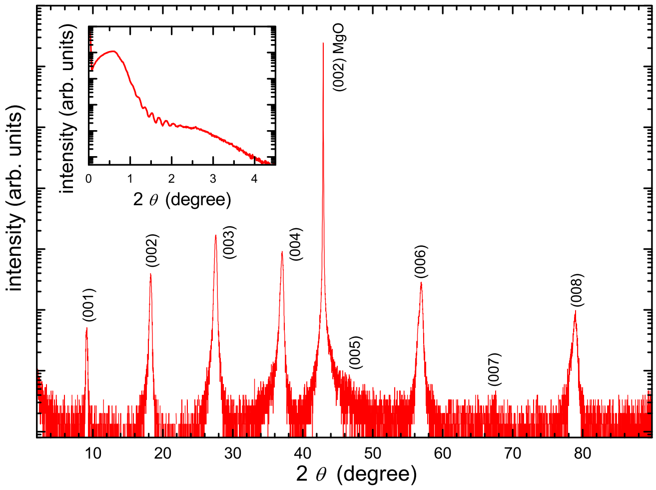

FIG. 9. (Color online) A 2θ-ω XRD scan of a $LaPd_xBi_2$ thin film. The intensities are shown on a logarithmic scale. Only $(00l)$ reflections are observed. The inset shows the XRR measurement.

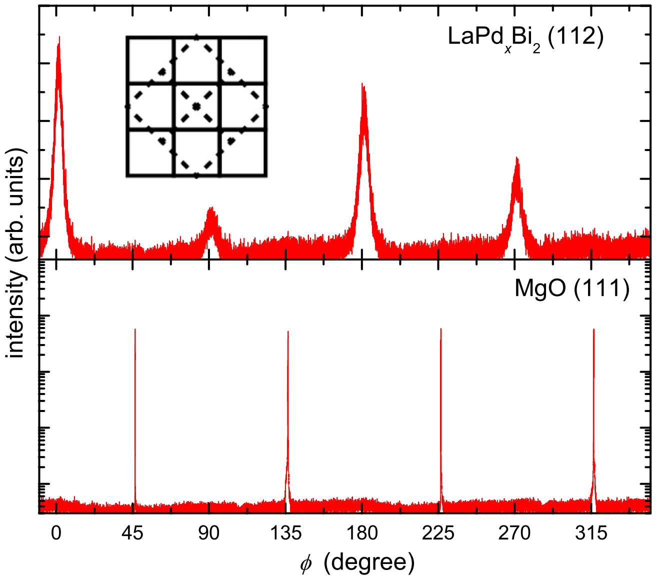

FIG. 10. (Color online) ϕ scan around the LaPd$_x$Bi$_2$ (112) reflection and the MgO (111) reflection. The drawing indicates the epitaxial relation. The unit cell of LaPd$_x$Bi$_2$ is represented by the dashed line; MgO is represented by a solid line.

of 0.44°. The inset of Fig. 9 shows a XRR measurement. The absence of clear Kiessig fringes shows that LaPd$_x$Bi$_2$ grows considerably less smooth than LaPd$_x$Sb$_2$. Note that the *in situ* surface of LaPd$_x$Bi$_2$ is atomically smooth (as indicated by RHEED observation); the surface roughening and film degradation are an effect of exposure to atmospheric conditions. In this study we have not used capping layers since we wanted to characterize the samples consistently including resistivity measurements.

We show the ϕ scans for LaPd$_x$Bi$_2$ (112) and MgO (111) in Fig. 10. The [110] direction of LaPd$_x$Bi$_2$ is parallel to [100] MgO, indicating that LaPd$_x$Bi$_2$ grows 45° rotated with respect to the cubic substrate. The intensities of the LaPd$_x$Bi$_2$ {112} peaks are not identical due to a bad sample in-plane alignment. A second measurement was not possible due to the fast degradation of the sample. The lattice mismatch to MgO is about 8.1%. We suggest that the bigger mismatch than that for LaPd$_x$Sb$_2$ results in the rotated growth mode, where a 2 × 2 cube of LaPd$_x$Bi$_2$ rotated 45° grows on top of a 3 × 3 cube of MgO unit cells with a lattice mismatch of 1.8% (see drawing in Fig. 10).

Figure 11 shows the temperature dependence of the resistivity for the LaPd$_x$Bi$_2$ thin film with the highest critical temperature. The superconducting onset starts at $T_c^{\text{onset}} = 3.03$ K, and the zero-resistivity value is at $T_c^{\text{zero}} = 2.70$ K, which is about 0.5 K below the best LaPd$_x$Sb$_2$ thin films. These values and the shape of $\rho(T)$ are in good agreement with single -crystal values for LaPd$_{0.85(2)}$Sb$_2$, where $T_c^{\text{zero}} = 2.1$ K. The small discrepancy in T_c^{zero} might be due to a difference in Pd occupation [17]. Despite the considerably faster degradation of the LaPd$_x$Bi$_2$ thin films, this 20% decrease in the transition temperature seems to be an intrinsic effect. If one assumes a BCS-type superconductivity in these compounds and that the main difference between Sb and Bi is the phonon frequencies, this is an expected result. The critical temperature is inversely proportional to the mass, and thus, the Sb-based compound is expected to have a higher T_c. In the range of 5 K to about 30 K, the resistivity shows a metallic behavior similar to that in the case of LaPd$_x$Sb$_2$, with a quadratic $\rho(T) = \rho_0 + AT^2$ dependence, with $\rho_0 = 86.6\,\mu\Omega\,\text{cm}$ and $A \approx 2.64\,\text{n}\Omega\,\text{cm/K}^2$. The resistivity at room temperature is $\rho(300\,\text{K}) = 150\,\mu\Omega\,\text{cm}$. The residual resistivity ratio is 1.70.

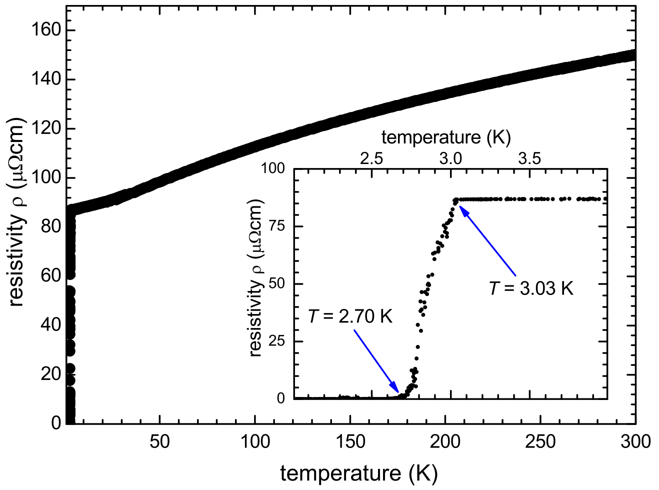

FIG. 11. (Color online) Temperature dependence of the resistivity of a LaPd$_x$Bi$_2$ thin film. The inset shows a zoom of the superconducting transition.

Experimentally, we do not observe that a change in the Pd concentration affects the transition temperature of LaPd$_x$Bi$_2$. There is a large plateau of constant T_c below 3 K. The data scatter is smaller than the scatter for individual Pd values. as shown in Fig. 12. For a high Pd rate, superconductivity breaks down completely at a certain threshold value. We assume that this transition is due to the structural instability of the compound. LaPd$_x$Bi$_2$ behaves analogous to LaPd$_x$Sb$_2$, where

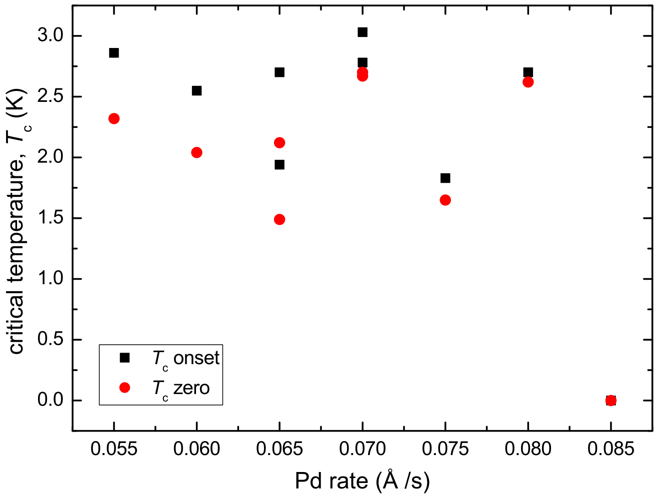

FIG. 12. (Color online) Phase diagram of LaPd$_x$Bi$_2$. Onset and zero-resistance values are shown.

the superconductivity also breaks down when the nominal stoichiometric compound is approached.

C. Microstructuring and critical currents in LaPd$_x$Sb$_2$

In order to estimate a typical critical current density in a microstructured conducting bridge of the 112 superconductors, we have chosen LaPd$_x$Sb$_2$ since it was more stable during the experiments. We have fabricated a microbridge with about 400 μm width by Ar ion-beam etching through a shadow mask. We have used 500 eV beam voltage and 10^{-3} A/cm^2 ion-beam density. Ion-beam etching has proven to be a suitable method for microstructuring in the case of high-temperature superconductors without inducing sample degradation [29]. In the case of LaPd$_x$Sb$_2$, the use of a shadow mask instead of electron-beam or photolithographic masks was necessary in order to avoid sample degradation due to the contact with photoresist. The disadvantage of this technique is the relatively large width of the superconducting bridge. Because of that, we have also used the focused ion beam (FIB) technique (at the Comenius University in Bratislava) to produce smaller bridges with a minimal width of 1.7 μm. However, this step already leads to optically visible sample degradation.

For the 400-μm-wide bridge, we have measured a critical current density of about 1.25×10^4 A/cm^2 at 0.38 K, which is three orders of magnitude below typical critical current densities for high-temperature superconducting cuprates but of the order of the critical current density in conventional metallic superconductors. Arsenic-containing Fe-based pnictide superconducting thin films show critical currents between 10^4 and 10^6 A/cm^2, depending on their structural details [30]. Note that during processing of the 400-μm microbridge, the T_c^{onset} of the material at the bridge was reduced to 2.6 K, with $T_c^{\text{zero}} = 2.2$ K (but not at the remaining unstructured parts of sample). The current-voltage characteristics of the wide microbridge as shown in Fig. 13 actually exhibit a behavior which is typical for a Josephson junction. This means that there is a weak link in the bridge area which could be due to a grain boundary. The weak-link critical-current value is therefore a lower limit to the bulk critical current of the compound itself in an ideal microbridge.

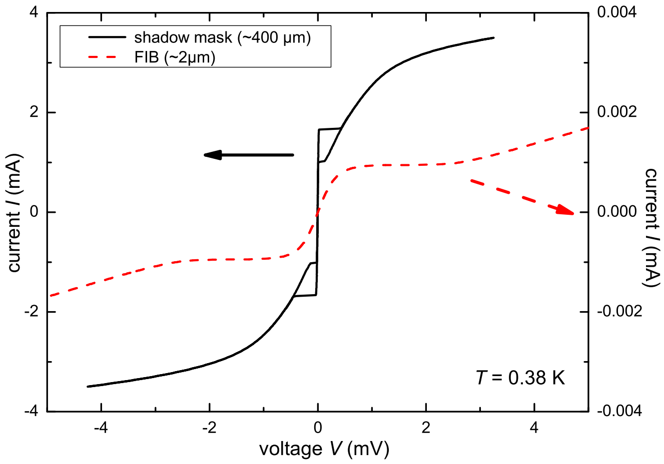

FIG. 13. (Color online) Current-voltage characteristics of a LaPd$_x$Sb$_2$ bridge with a width of 400 μm (solid black line) and of a microbridge with a width of 1.7 μm (dashed red line) measured at 0.38 K.

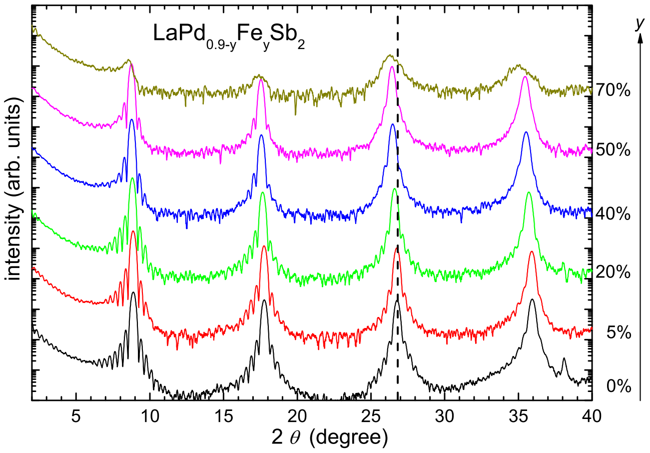

FIG. 14. (Color online) Comparison of 2θ-ω XRD scans of LaPd$_{0.9-y}$Fe$_y$Sb$_2$ with $0 \leqslant y \leqslant 0.7$.

D. Effect of Fe substitution in LaPd$_x$Sb$_2$

In a conventional superconductor, the addition of Fe typically leads to a fast suppression of superconductivity due to the antagonism of superconductivity and magnetic impurities. Since it is extremely challenging to replace Pd completely by Fe, we have started to substitute Pd by Fe in the more stable compound LaPd$_x$Sb$_2$. In total, we have grown five samples with different Fe contents on MgO substrates with the chemical formula LaFe$_y$Pd$_{0.9-y}$Sb$_2$ with $0 \leqslant y \leqslant 0.7$. Figure 14 shows the evolution of 2θ-ω XRD scans with increasing Fe substitution. Fe can be substituted with reasonable crystallinity up to about 50%. For $y = 0.7$ the crystallinity is drastically reduced, and the compound becomes structurally unstable. There is an overall reduction in crystallinity with increasing y. Nevertheless, for $y < 0.7$ Laue oscillations could be observed up to $y \approx 0.5$. Most important, the shift of the angle of the (003) peak clearly demonstrates the substitution of Pd by Fe and a corresponding increase of the lattice constant, which is shown in Fig. 15. The almost linear behavior is compatible with Vegard's law. The key result is that in all Fe-substituted samples superconductivity is completely suppressed. The resistivity behavior is semiconducting rather than metallic.

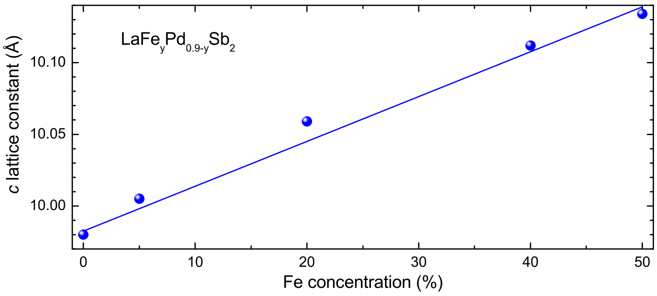

FIG. 15. (Color online) The c-axis lattice constant of Pd$_{0.9-y}$Fe$_y$Sb$_2$ obtained using the Nelson-Riley method as a function of y.

Even a small amount of Fe scatterers of 5% is enough to kill the superconducting state. This behavior is typical for conventional superconductors where magnetic impurities breaking time-reversal symmetry are known to strongly reduce the critical temperature due to a modification of the BCS density of states. The critical value of magnetic impurities after which superconductivity is completely destroyed is obviously reached in $\text{LaPd}_{0.9-y}\text{Fe}_y\text{Sb}_2$ already for $y < 0.05$. From this experiment we conclude that LaPd_xSb_2 and LaPd_xBi_2 are conventional s-wave superconductors. The fact that iron impurities are that effective in the suppression of superconductivity indicates that the superconducting layer is the Pd(Fe)-Pn layer where the Fe substitutes Pd. If the superconductivity originated in the two-dimensional pnictide square net layer, the effect of Fe doping would be less pronounced.

IV. CONCLUSION

The 112-pnictide superconductors are a subgroup of pnictides with a peculiar structural feature, which is the pnictide square net layer. We have chosen a thin-film approach using MBE to obtain epitaxial and phase-pure thin films of $\text{LaPd}_x Pn_2$ ($Pn = \text{Sb, Bi}$) grown on (100) MgO substrates. The occupation of Pd, which is typically below 1 ($x < 1$), almost does not affect superconductivity, which is suppressed only when the structural stability of the compound is weakened. The Sb-based compound has a higher critical temperature ($T_c = 3.2$ K) than the Bi-based compound ($T_c = 2.7$ K), in agreement with a phonon-mediated superconductivity scenario. The assumption of a conventional BCS-type superconductivity is further corroborated by the fast suppression of superconductivity upon magnetic substitution of Pd by Fe.

ACKNOWLEDGMENTS

This work was supported by the Deutsche Forschungsgemeinschaft (DFG) through Grant No. SPP 1458 (LA 560/10-2 and SE 664/15-2). We thank T. Plecenik and M. Tomášek of Comenius University in Bratislava for the FIB preparation. We also thank S. Döring, V. Tympel, S. Gottwals, and O. Krško for their technical assistance. This work was partially supported by the Landesgraduiertenförderung Thüringen.

[1] V. Johnson and W. Jeitschko, J. Solid State Chem. **11**, 161 (1974).

[2] Y. Kamihara, T. Watanabe, M. Hirano, and H. Hosono, J. Am. Chem. Soc. **130**, 3296 (2008).

[3] H. Takahashi, K. Igawa, K. Arii, Y. Kamihara, M. Hirano, and H. Hosono, Nature (London) **453**, 376 (2008).

[4] Z.-A. Ren, J. Yang, W. Lu, W. Yi, X.-L. Shen, Z.-C. Li, G.-C. Che, X.-L. Dong, L.-L. Sun, F. Zhou, and Z.-X. Zhao, Europhys. Lett. **82**, 57002 (2008).

[5] J. H. Shim, K. Haule, and G. Kotliar, Phys. Rev. B **79**, 060501(R) (2009).

[6] Y.-Z. Zhang, I. Opahle, H. O. Jeschke, and R. Valentí, Phys. Rev. B **81**, 094505 (2010).

[7] N. Katayama, K. Kudo, S. Onari, T. Mizukami, K. Sugawara, Y. Sugiyama, Y. Kitahama, K. Iba, K. Fujimura, N. Nishimoto, M. Nohara, and H. Sawa, J. Phys. Soc. Jpn. **82**, 123702 (2013).

[8] K. Kudo, T. Mizukami, Y. Kitahama, D. Mitsuoka, K. Iba, K. Fujimura, N. Nishimoto, Y. Hiraoka, and M. Nohara, J. Phys. Soc. Jpn. **83**, 025001 (2014).

[9] K. Kudo, Y. Kitahama, K. Fujimura, T. Mizukami, H. Ota, and M. Nohara, J. Phys. Soc. Jpn. **83**, 093705 (2014).

[10] W. Zhou, J. Zhuang, F. Yuan, X. Li, X. Xing, Y. Sun, and Z. Shi, Appl. Phys. Express **7**, 063102 (2014).

[11] A. Sala, H. Yakita, H. Ogino, T. Okada, A. Yamamoto, K. Kishio, S. Ishida, A. Iyo, H. Eisaki, M. Fujioka, Y. Takano, M. Putti, and J.-I. Shimoyama, Appl. Phys. Express **7**, 073102 (2014).

[12] L. S. Andrukhiv, L. A. Lysenko, Ya. P. Yarmolyuk, and E. I. Gladyshevskii, Dopov. Akad. Nauk Ukr. RSR, Ser. A: Fiz.-Tekh. Mat. Nauki **7**, 645 (1975).

[13] M. Brylak, M. H. Möller, and W. Jeitschko, J. Solid State Chem. **115**, 305 (1995).

[14] H. Mizoguchi, S. Matsuishi, M. Hirano, M. Tachibana, E. Takayama-Muromachi, H. Kawaji, and H. Hosono, Phys. Rev. Lett. **106**, 057002 (2011).

[15] K. Kodama, S. Wakimoto, N. Igawa, S. Shamoto, H. Mizoguchi, and H. Hosono, Phys. Rev. B **83**, 214512 (2011).

[16] L. Schoop, D. Hirai, C. Felser, and R. J. Cava, Europhys. Lett. **101**, 67001 (2013).

[17] F. Han, C. D. Malliakas, C. C. Stoumpos, M. Sturza, H. Claus, D. Y. Chung, and M. G. Kanatzidis, Phys. Rev. B **88**, 144511 (2013).

[18] L. Alff, A. Klein, P. Komissinskiy, and J. Kurian, in *Ceramic Science and Technology*, edited by I.-W. Chen and R. Riedel (Wiley-VCH, Weinheim, 2011), Vol. 3, pp. 267–289.

[19] J. Kurian, A. Buckow, R. Retzlaff, and L. Alff, Phys. C (Amsterdam, Neth.) **484**, 171 (2013).

[20] A. Buckow, K. Kupka, R. Retzlaff, J. Kurian, and L. Alff, Appl. Phys. Lett. **101**, 162602 (2012).

[21] A. Buckow, R. Retzlaff, J. Kurian, and L. Alff, Supercond. Sci. Technol. **26**, 015014 (2013).

[22] Y. Muro, N. Takeda, and M. Ishikawa, J. Alloys Compd. **257**, 23 (1997).

[23] V. K. Anand, H. Kim, M. A. Tanatar, R. Prozorov, and D. C. Johnston, Phys. Rev. B **87**, 224510 (2013).

[24] T. K. Kim, A. N. Yaresko, V. B. Zabolotnyy, A. A. Kordyuk, D. V. Evtushinsky, N. H. Sung, B. K. Cho, T. Samuely, P. Szabó, J. G. Rodrigo, J. T. Park, D. S. Inosov, P. Samuely, B. Büchner, and S. V. Borisenko, Phys. Rev. B **85**, 014520 (2012).

[25] S. Ganesanpotti, T. Yajima, T. Tohyama, Z. Li, K. Nakano, Y. Nozaki, C. Tassel, Y. Kobayashi, and H. Kageyama, J. Alloys Compd. **583**, 151 (2014).

[26] A. Leithe-Jasper and P. Rogl, J. Alloys Compd. **203**, 133 (1994).

[27] H. Zama, Y. Ishii, H. Yamamoto, and T. Morishita, Jpn. J. Appl. Phys. **40**, L465 (2001).

[28] J. B. Nelson and D. P. Riley, Proc. Phys. Soc. London **57**, 160 (1945).

[29] L. Alff, G. M. Fischer, R. Gross, F. Kober, A. Beck, K. D. Husemann, T. Nissel, F. Schmidl, and C. Burckhardt, Phys. C (Amsterdam, Neth.) **200**, 277 (1992).

[30] S. Haindl, M. Kidszun, S. Oswald, C. Hes, B. Büchner, S. Kölling, L. WIlde, T. Thersleff, V. V. Yurchenko, M. Jourdan, H. Hiramatsu, and H. Hosono, Rep. Prog. Phys. **77**, 046502 (2014).